Electronic Supplementary Material (ESI) for Nanoscale.

Supporting Information

Topological defects involving Fe/N co-doped mesoporous carbon nanosheets as novel electrocatalysts for the oxygen reduction reaction and Zn–air batteries

Junjie Ding,[a,b] *Dongchuang Wu,*[a,b] *Senhe Huang,*[b] *Chenbao Lu,*[b] *Yu Chen,**[a] *Jichao Zhang,*[e] *Longhai Zhang,*[c] *Jin Li,*[c,d] *Changchun Ke,**[c] *Diana Tranca,*[b] *Emmanuel Kymakis,*[f] *Xiaodong Zhuang**[b]

[a] Key Lab for Advanced Materials, Institute of Applied Chemistry, East China University of Science and Technology,130 Meilong Road, Shanghai 200237, China.
[b] The meso-Entropy Matter Lab, State Key Laboratory of Metal Matrix Composites, Shanghai Key Laboratory of Electrical Insulation and Thermal Ageing, School of Chemistry and Chemical Engineering, Shanghai Jiao Tong University, 800 Dongchuan Road, Shanghai 200240, China.
[c] Institute of Fuel Cells, School of Mechanical Engineering, Shanghai Jiao Tong University, 800 Dongchuan Road, Shanghai 200240, China.
[d] Henan Engineering Technology Research Center of Fuel Cell and Hydrogen Energy, Zhengzhou Yutong Bus Co. Ltd, Yuxing Road, Zhengzhou 451472, China.
[f] Shanghai Synchrotron Radiation Facility, Zhangjiang Laboratory, Shanghai Advanced Research Institute, Chinese Academy of Sciences, No. 239, Zhangheng Road, Shanghai 201204, China.
[e] Department of Electrical & Computer Engineering, Hellenic Mediterranean University, 71410 Heraklion, Greece.

Table of Contents

1. Experimental Section

Chemicals: Tropolone, tosyl chloride, ethyl cyanacetate, pyridine and sodium ethoxide were purchased from Aladdin Reagent Co. Ammonium peroxydisulfate (APS), HCl (36 wt%), $KMnO_4$, $NaNO_3$, NaOH, $FeCl_3$, triethylamine and H_2O_2 were purchased from Sinopharm Chemical Reagent Co. Pt/C (20 wt%) was purchased from Sigma-Aldrich. Nafion solution (5 wt%) was purchased from DuPont, Ltd. All chemicals were used without further purification. 2-aminoazulene was synthesized by a reported method.[1] Graphene oxide (GO) was synthesized from natural flake graphite by a modified Hummers method.[2] Silica spheres assembled GO was synthesized according literature.[3]

Preparation of GPAz: Poly(2-aminoazulene) functionalized graphene oxide nanosheets were prepared by in-situ polymerization of 2-aminoazulene on GO-SS. Firstly, GO-SS (66 mg) and ammonium persulfate (3 g, 13.1 mmol) was transferred into a 2 L round-bottomed flask. After adding deionized water (1L) and ultrasonication for 30 min to form a homogeneous suspension, 2-aminoazulene (1 g, 7.0 mmol), dissolved in 1 M HCl (250 mL), was added dropwise to the above GO suspension. The mixture was vigorously stirred overnight. Then, the resulting gray suspension was filtrated and washed with deionized water for three times to obtain GPAz-SS. GPANI-SS was obtained by the same procedure using aniline instead of 2-aminoazulene. PAz-SS was obtained by the same procedure using silica spheres as template instead of silica spheres assembled GO. PAz was synthesized by direct polymerization of 2-aminoazulene without using any templates.

Preparation of mPCN-Fe: Firstly, $FeCl_3$ (100 mg 0.62 mmol) was dissolved in 30 mL deionized water and added into *GPAz-SS* (200 mg). The mixture was vigorously stirred overnight. Subsequently, the mixture was filtered and dried in oven followed by grinding into fine powder. Then, after carbonized at 800-1000 ℃ under Ar atmosphere for 2 h at the heating rate of 5 ℃ min^{-1} and followed by treating in NH_3 atmosphere for 10 min, Fe/N co-doped porous carbon nanosheets can be produced (800 ℃: mPCN-Fe-800 (yield: 60%) ; 900 ℃: mPCN-Fe (yield: 52%); 1000 ℃: mPCN-Fe-1000 (yield: 43%)). As control experiment, mPCN-Fe' and mPCN-Fe'-T (T=800, 1000), mPC-Fe and mPC-Fe-T (T=800, 1000), PC-Fe and PC-Fe-T (T=800, 1000) was fabricated in the same way using GPANI-SS, PAz-SS and PAz as starting materials, respectively.

Characterizations: SEM measurements were performed on a Nova NanoSEM 450 field emission scanning electron microscope. TEM images were acquired using a TALOS F200X field emission transmission electron microscope operated at 200 kV. AFM images of the materials on a freshly cleaved mica surface were taken with a Nanoscope III in tapping mode using a NSC14/no Alprobe (MikroMash, Wislson-ville, Oregen). XRD analysis was performed on a D8 Advance X-ray diffractometer with Cu Kα radiation (k = 1.54 Å) at a generator voltage of 40 kV and a generator current of 40 mA with a scanning speed of 6° min^{-1} over the range 5−80° (2θ). The Raman spectra of samples were obtained on Lab-RAM HR800 with excitation by an argon ion laser (532 nm). TGA of the samples was performed using a Q5000IR (TA Instruments, USA) thermogravimetric analyzer at a heating rate of 20 °C min^{-1} under nitrogen flow. X-ray photoemission spectroscopy (XPS) measurements were performed on a *1/AXIS Ultra DLD system; the C 1s value was set at 284.8 eV for charge corrections. The gas sorption isotherms were measured via an Autosorb-iQA3200-4 sorption analyzer (Quantatech Co., USA) based on N_2 adsorption/desorption.

2. Electrochemical Measurements

The work electrode was prepared by loading a catalyst sample film of 0.36 mg cm^{-2} onto a glass carbon electrode (0.2471 cm^2). Firstly, 5 mg catalyst was dispersed in 500 μL 0.5% Nafion ethanol solution. After stirring overnight and sonicating for 30 min, the mixture formed a homogeneous dispersion. Then, 9 μL catalyst ink was loaded on the surface of glassy carbon electrode and dried at the room tempetature.

Cyclic voltammetry, rotating disk electrode (RDE) and rotating ring-disk electrode (RRDE) measurements were performed a basic bipotentiostat (Pine Research Instrumentation, USA) with a three electrode cell system. A rotating glass carbon disk and platinum ring electrode loaded the catalyst was used as the working electrode, an Ag/AgCl (KCl, 3 M) electrode and a Pt wire were used as the reference electrode and the counter electrode, respectively. The electrochemical experiments were conducted in O_2 saturated 0.1 M KOH and 0.5 M H_2SO_4 electrolyte for the oxygen reduction reaction. The potential range was cyclically scanned from 0.1 V to −1 V at a scan rate of 100 mV/s at the room temperature. RDE measurements were conducted at different rotating speeds from 225 to 2500 rpm at a scan rate of 10 mV/s. The potential measured against Ag/AgCl was converted to a RHE by equation 1:

$$E(RHE) = E(Ag/AgCl)+0.059 \times [PH]+0.2046. \tag{1}$$

Based on the RRDE result, the H_2O_2 (%) and the electron transfer number (n) were determined bythe following equations:

$$n = \frac{4I_D}{I_D + I_R/N} \tag{2}$$

$$H_2O_2 = \frac{200I_R/N}{I_D + I_R/N} \tag{3}$$

where I_D is disk current, I_R is ring current, and N is current collection efficiency of the Pt ring, which was provided as 0.37 by manufacture.

The transferred electron number (n) per oxygen molecule in the ORR process at electrode can be calculated by the Koutechy–Levich (K–L) equations (4-6).

$$\frac{1}{J} = \frac{1}{J_L} + \frac{1}{J_K} = \frac{1}{B\omega^{1/2}} + \frac{1}{J_K} \tag{4}$$

$$B = 0.2nFC_0D_0^{2/3}v^{-1/6} \tag{5}$$

$$J_K = nfKC_0 \tag{6}$$

in which J is the measured current density, J_K and J_L are the kinetic- and diffusion-limiting current densities, μ is the angular velocity of the rotating electrode ($\omega=2\pi N$, N is the linear rotation speed), F is the Faraday constant (F = 96485 C mol^{-1}), C_0 is the concentration of O_2, D_0 is the diffusion coefficient of O_2, ν is the kinematic viscosity of the electrolyte, and k is the electron transfer rate constant. Since the electrolyte is O_2 saturated 0.1 M KOH, C_0, D_0 and v are constant as 1.2×10^{-3} M, 1.9×10^{-5} cm^2 s^{-1}, and 0.01 cm^2 s^{-1}, respectively.

Chronoamperometric responses of mPCN-Fe, and Pt/C were performed at 0.2 V (vs Ag/AgCl) in O_2-saturated 0.1 m KOH solutions at the rotation of 1600 rpm for 600 s with the introduction of methanol (3.0 m) at 300 s.

Zn-air batteries: Primary and rechargeable Zn–air batteries were tested in laboratory-constructed electrochemical cells. 5 mg catalyst was dispersed in 500 μL 0.5% of Nafion solution to form the catalyst ink. A Zn foil (3.45 g) and carbon paper loaded 100 μL catalyst ink with area of 1 cm^2 were used as the anode and cathode, respectively. Then, 35 mL of 6.0 M KOH with 0.1 M $ZnCl_2$ was used as electrolyte. Nickel foam was used as the current collector. Pt/C based Zn-air battery was measured in the same condition. Polarization curves was measured on CHI 660D electrochemical workstation. Other measurements was performed on LAND CT2001A battery testing system.

3. DFT calculations

DFT calculations have been performed using the Vienna *ab* initio simulation package (VASP)[1] with the projector-augmented wave (PAW)[2] method. All calculations were based on the same generalized gradient approximation (GGA) method with Perdew-Burke-Ernzerhof (PBE)[3] functional for the exchange-correlation term. The plane wave cutoff was set to 400 eV. The Brillouin zone integration was carried out with 2×2×1 Monkhorst-Pack *k*-point grid. The convergence of energy and forces were set to 5×10^{-4} eV and 0.01 eV $Å^{-1}$, respectively. A periodically repeated single-layer graphene model with C_{57} defects and Fe-N_4 structures embedded in the in-plane matrix has been built to simulate the Fe/N co-doped catalysts with a vacuum slab height of 20 Å, the graphene model doped with N only has also been studied. All atoms of the catalysts and adsorbates were fully relaxed during calculations. The free energy of each species is calculated by: $G = E^{DFT} + ZPE - T\Delta S$, where E^{DFT} is the DFT-optimized total energy, ZPE is the zero-point vibrational energy, T is the temperature, and ΔS is the entropy).

The zero-point energies and entropies of the reaction species were calculated from the vibrational frequencies. During these frequency calculations, all atoms of substrate were rigidly constrained so that no additional degrees of freedom, due to the catalyst, are introduced in to the reacting system. The thermodynamic quantities for the CO_2, CO, H_2O and H_2 species in the gas phase and reaction intermediates are shown in Table S1.

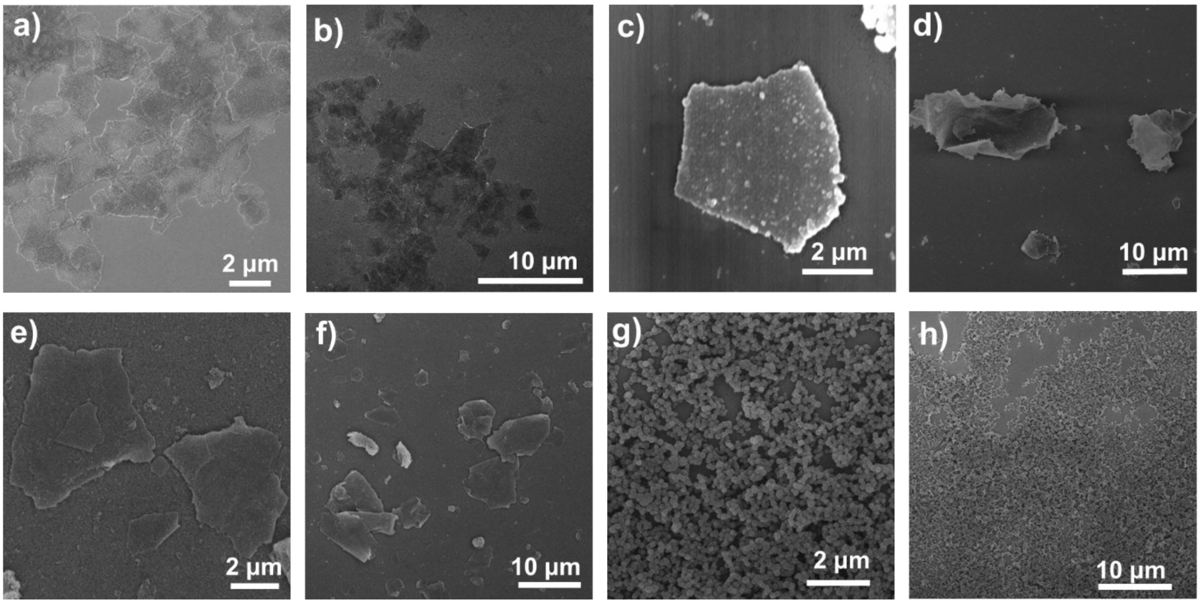

Figure S1. SEM images of (a-b) GO-SS, (c-d) GPAz-SS, (e-f) GPANI-SS and (d-h) PAz-SS.

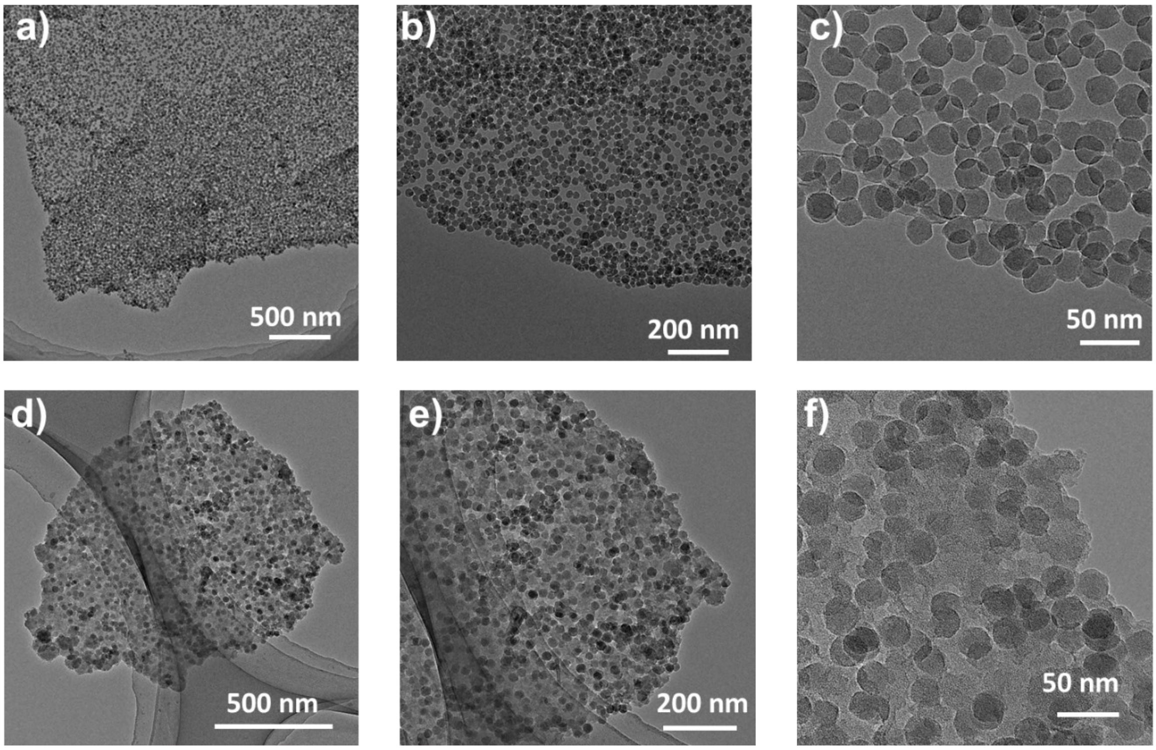

Figure S2. TEM images of (a-c) GO-SS and (d-f) GPAz-SS.

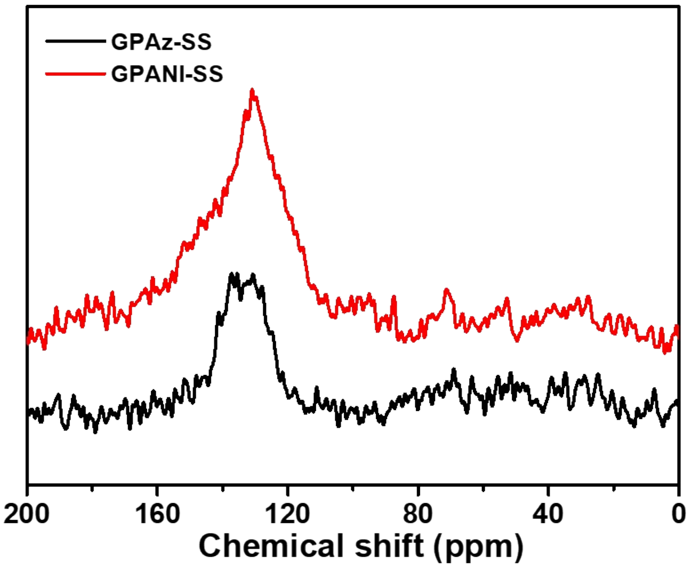

Figure S3. Solid-^{13}C NMR spectra of GPAz-SS and GPANI-SS.

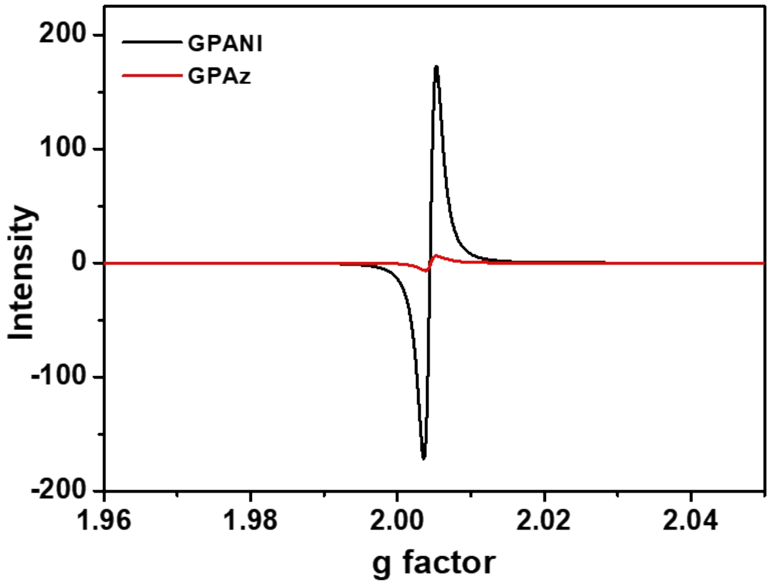

Figure S4. EPR spectra of GPAz and GPANI.

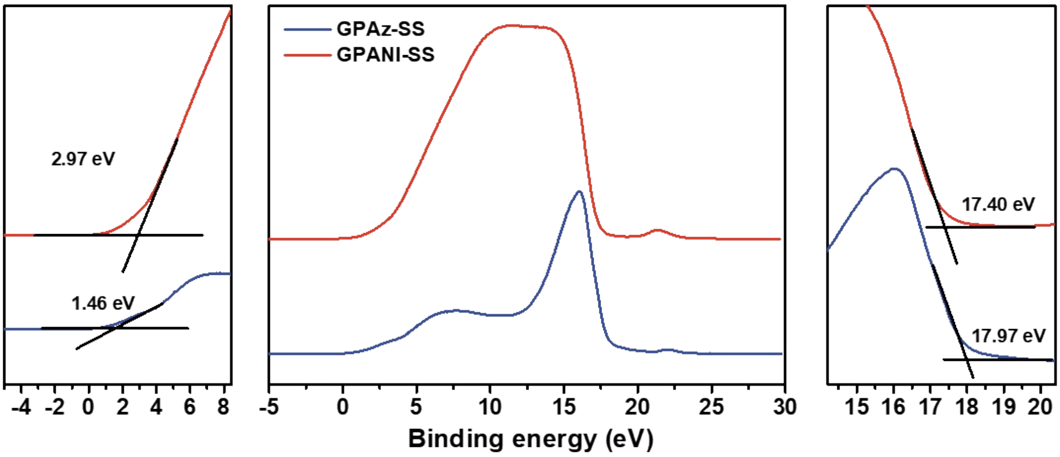

Figure S5. UPS spectra of GPAz-SS and GPANI-SS.

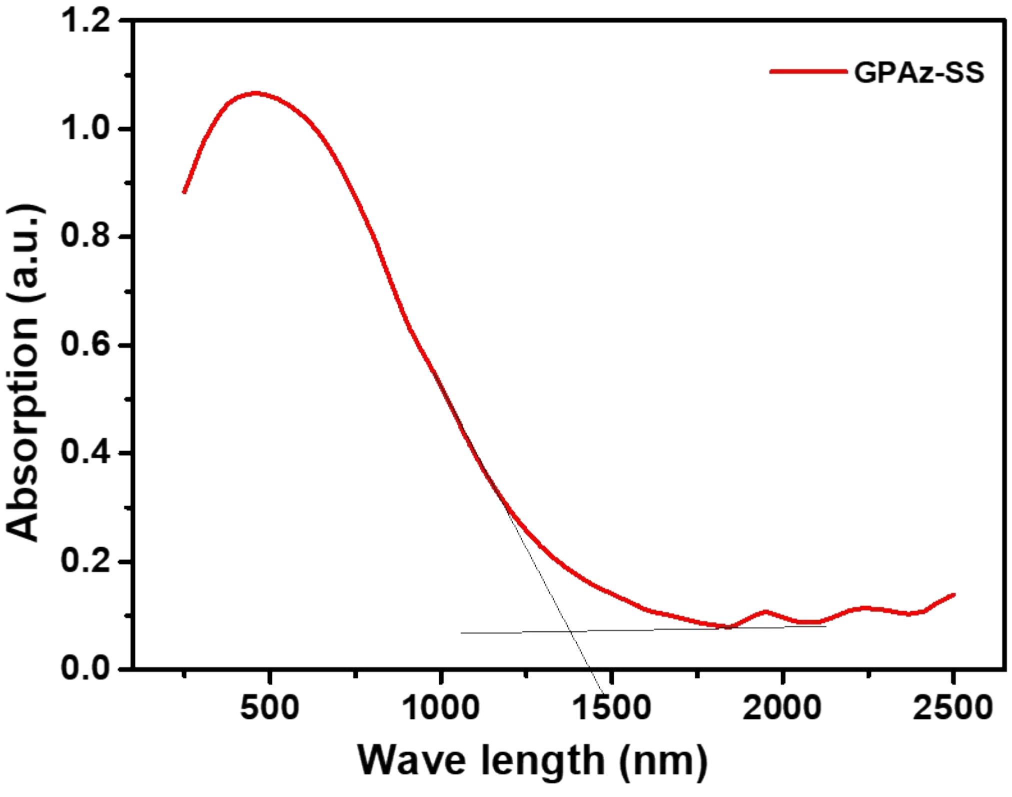

Figure S6. Solid-UV-vis spectrum of GPAz-SS.

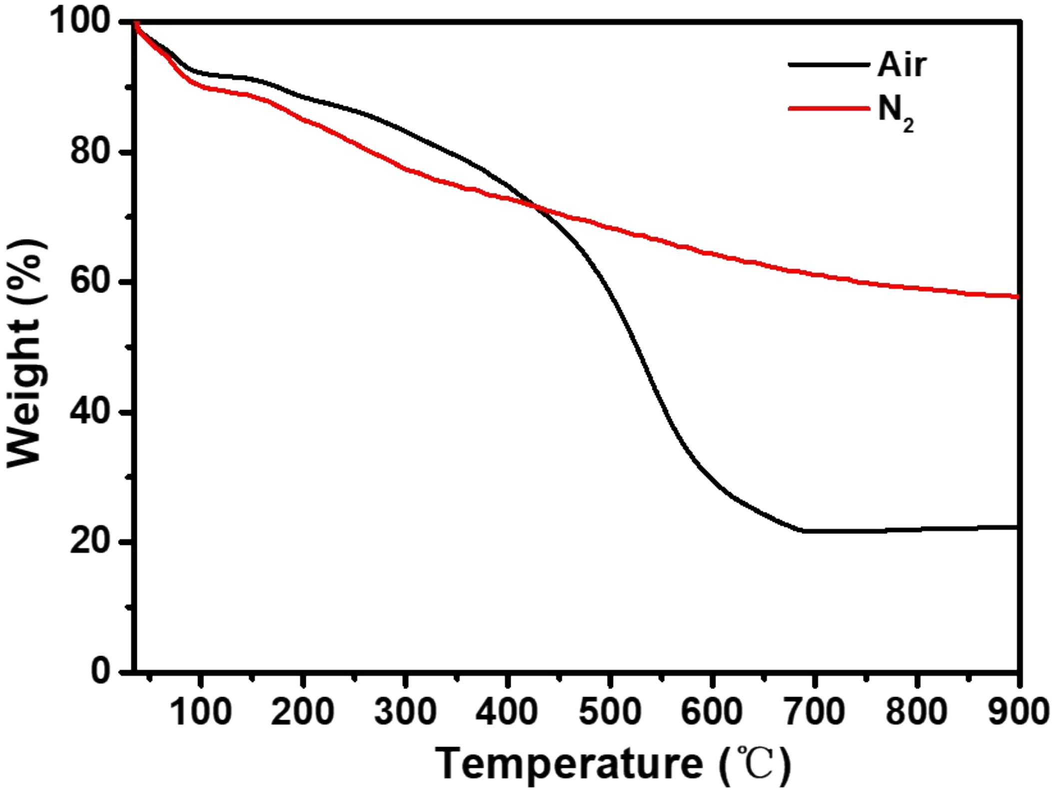

Figure S7. TGA curves of GPAz in the air and N_2 atmosphere.

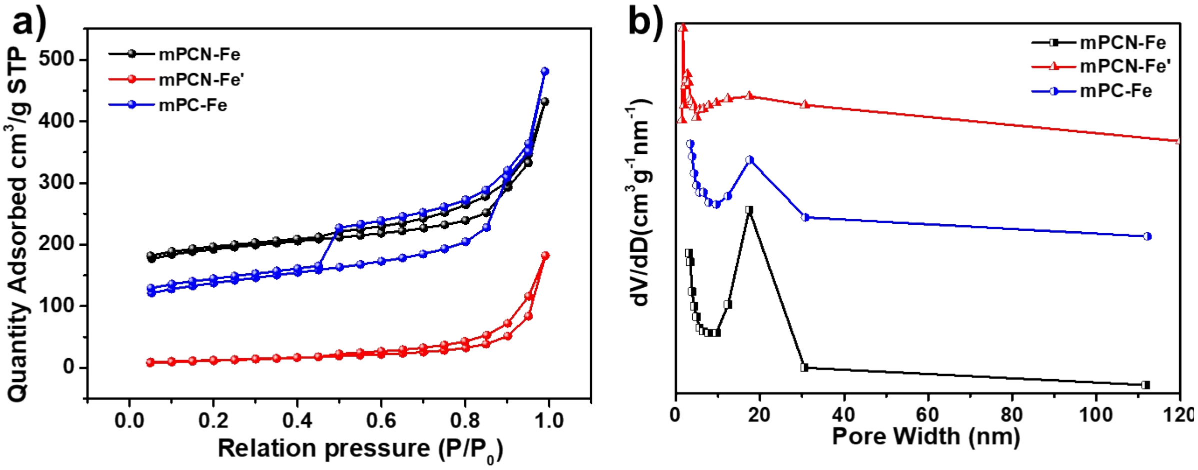

Figure S8. a) N_2 sorption isotherms and b) pore size distributions of mPCN-Fe, mPCN-Fe' and PC-Fe.

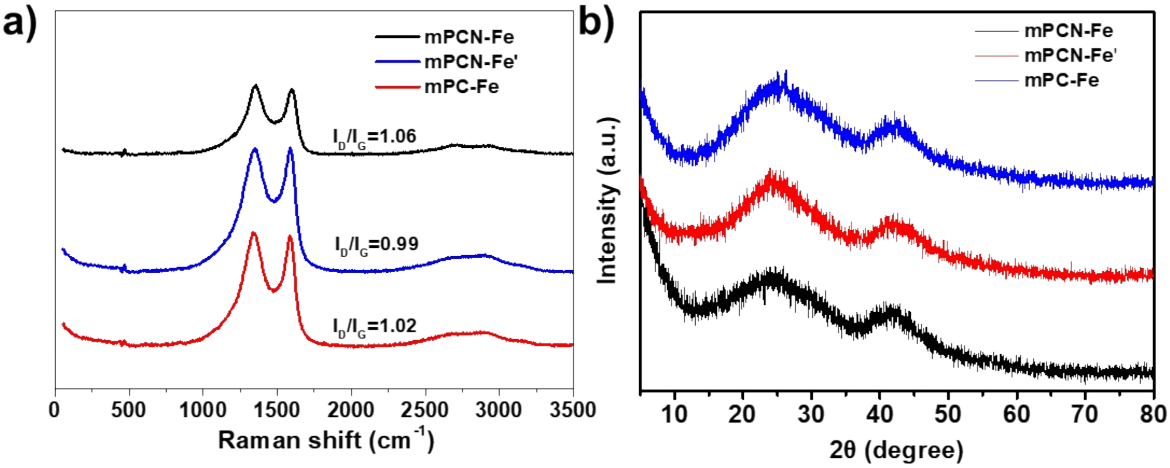

Figure S9. a) Raman curves and b) XRD patterns of mPCN-Fe, mPCN-Fe' and mPC-Fe.

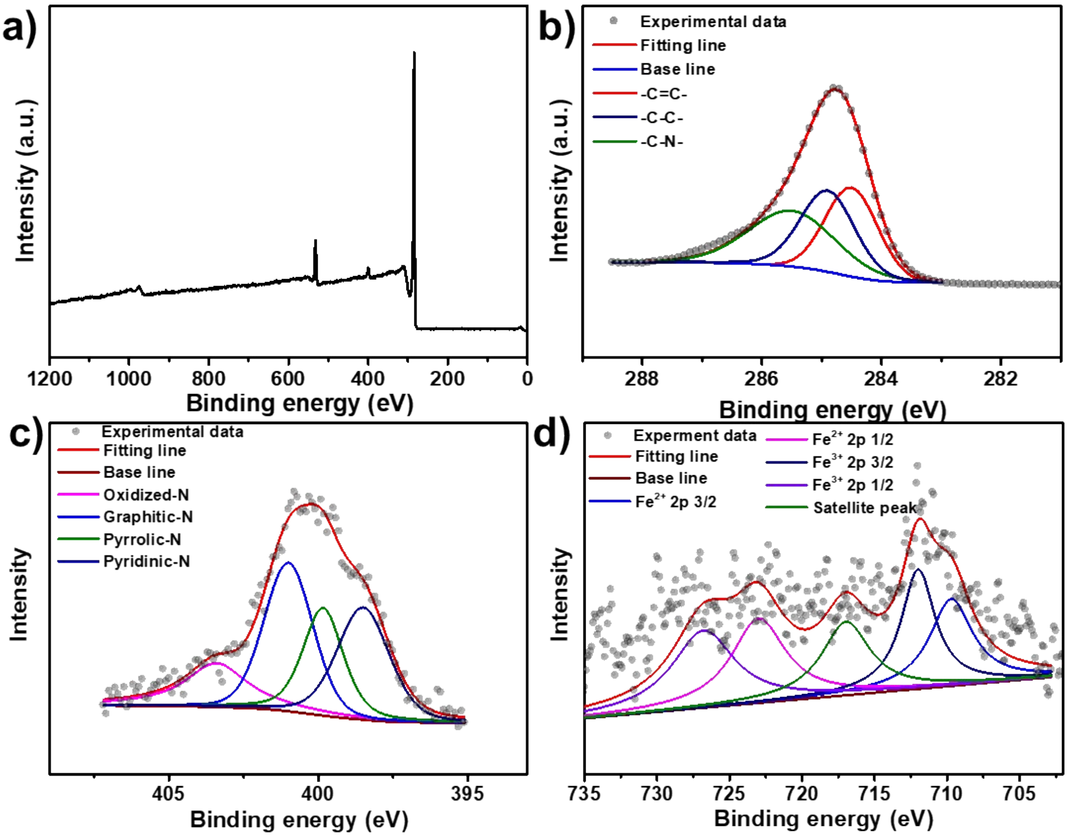

Figure S10. a) XPS spectrum, b) C 1s, c) N 1s, and d) Fe 2p XPS core level regions of mPCN-Fe.

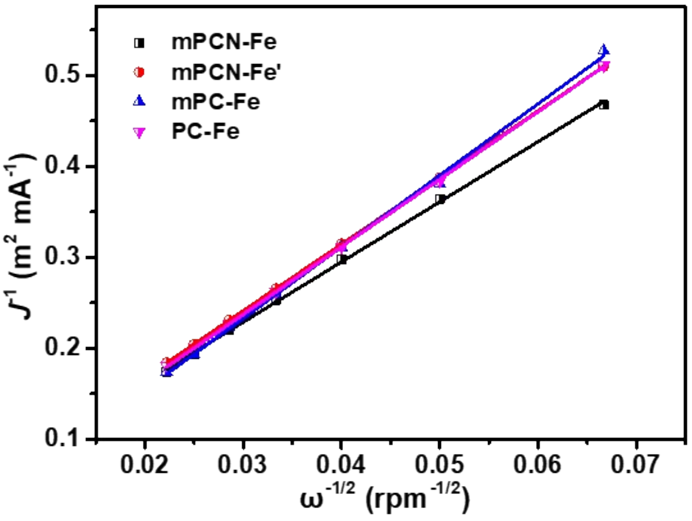

Figure S11. K-L plots of mPCN-Fe, mPCN-Fe’, mPC-Fe, and PC-Fe at 0.4 V.

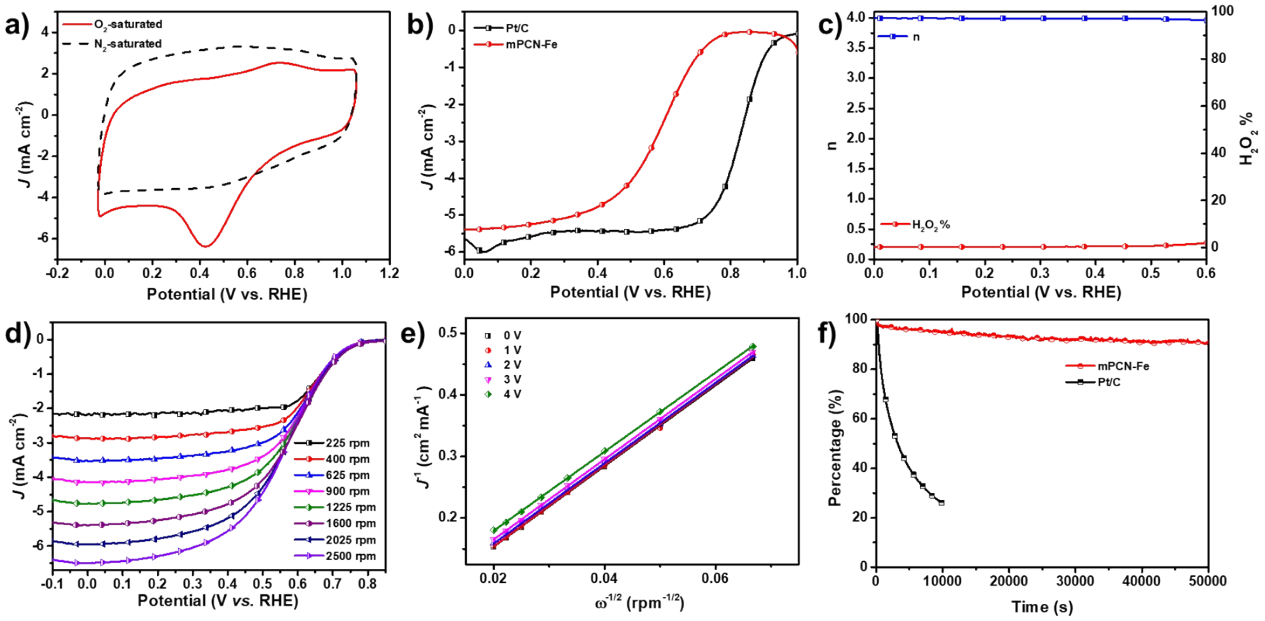

Figure S12. a) CV curves mPCN-Fe measured in N_2- and O_2-saturated 0.1 M $HClO_4$ solution at a scan rate of 100 mV s^{-1}. b) LSV curves of mPCN-Fe and Pt/C at a rotating rate of 1600 rpm. c) Calculated electron transfer number (n) and H_2O_2 yield of mPCN-Fe. d) LSV curves of mPCN-Fe at different rotation rate. e) Corresponding Koutecky–Levich plots at different potential. f) Long time stability of mPCN-Fe and Pt/C.

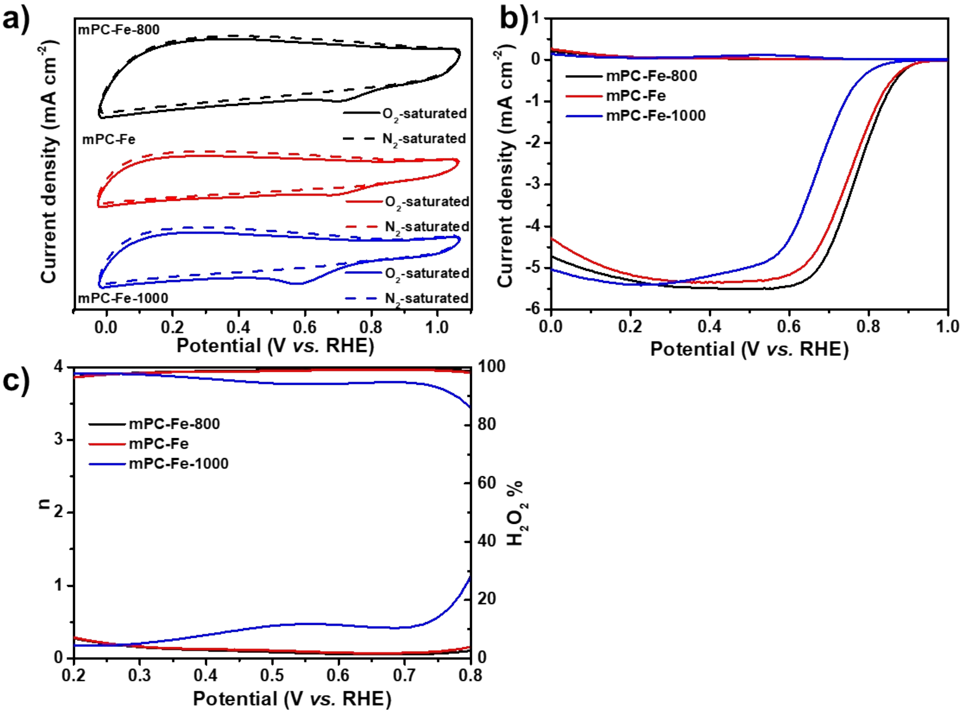

Figure S13. a) CV curves, b) RRDE curves and c) calculated electron transfer number and H_2O_2 yield of mPC-Fe-800, mPC-Fe, and mPC-Fe-1000.

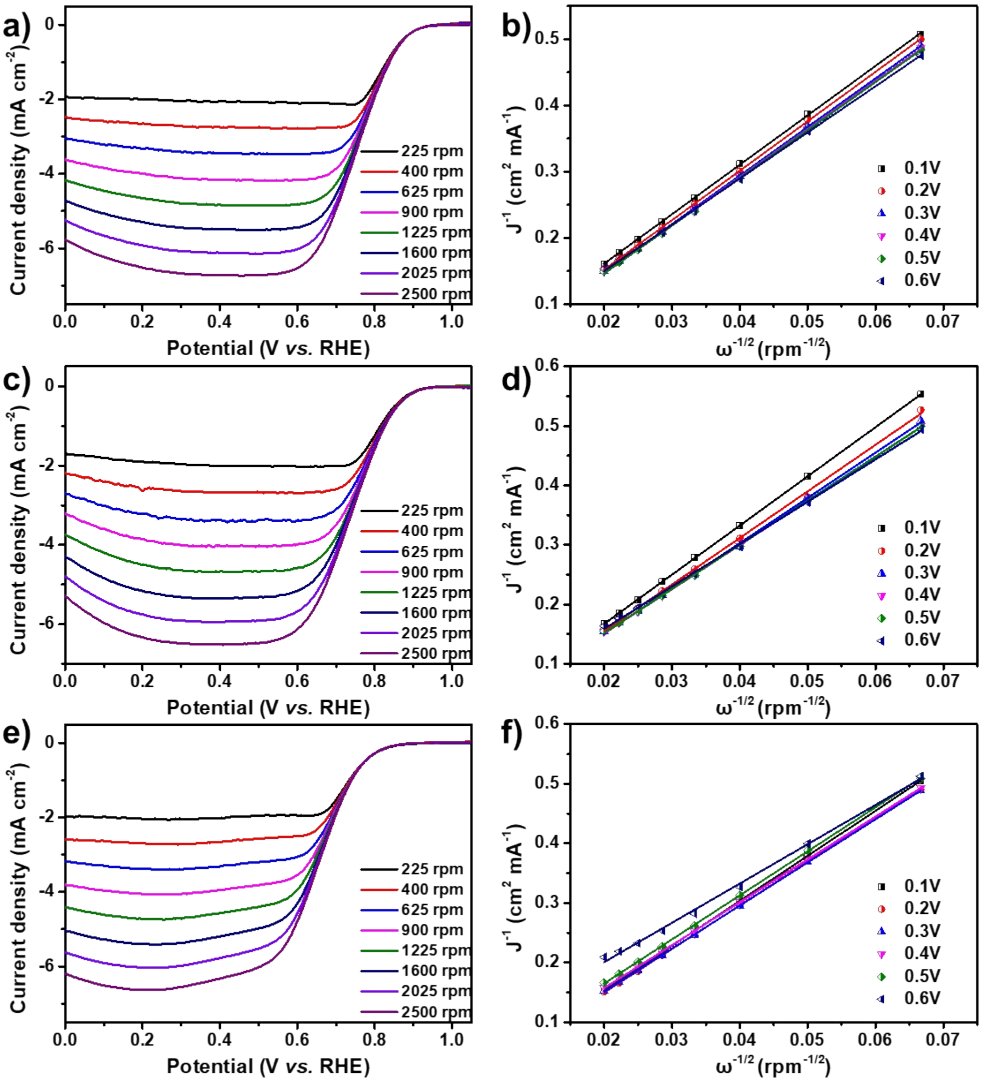

Figure S14. a) LSV curves at different rotation speeds (225–2025 rpm) and b) K-L plots of mPC-Fe-800. c) LSV curves at different rotation speeds (225–2025 rpm) and d) K-L plots of mPC-Fe. e) LSV curves at different rotation speeds (225–2025 rpm) and f) K-L plots of mPC-Fe-1000.

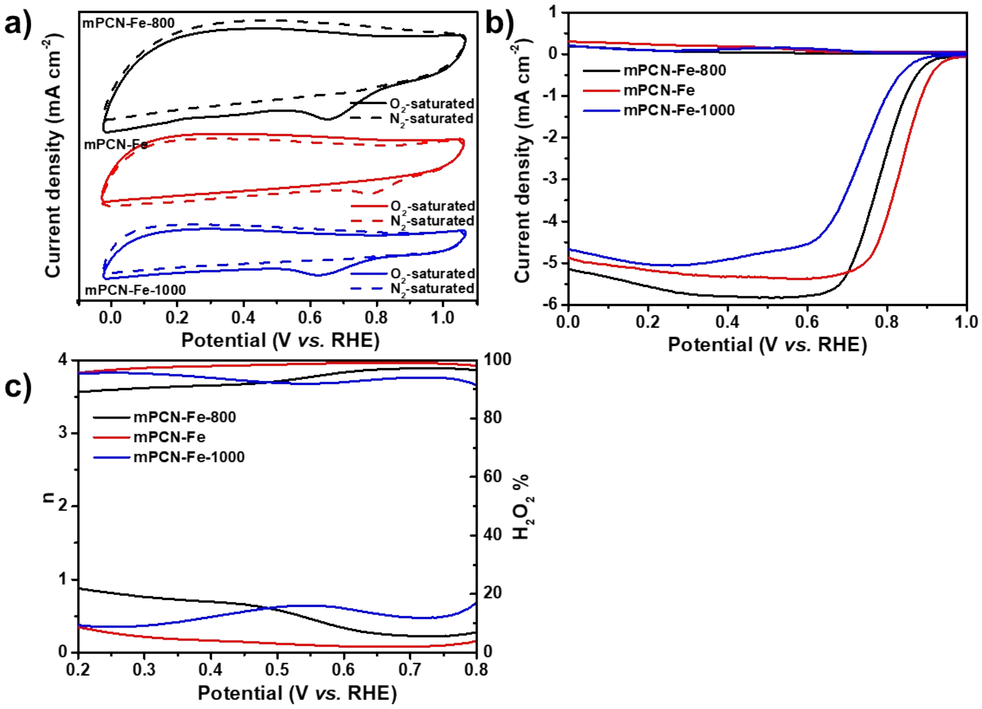

Figure S15. a) CV curves, b) RRDE curves and c) calculated electron transfer number and H_2O_2 yield of mPCN-Fe-800, mPCN-Fe, and mPCN-Fe-1000.

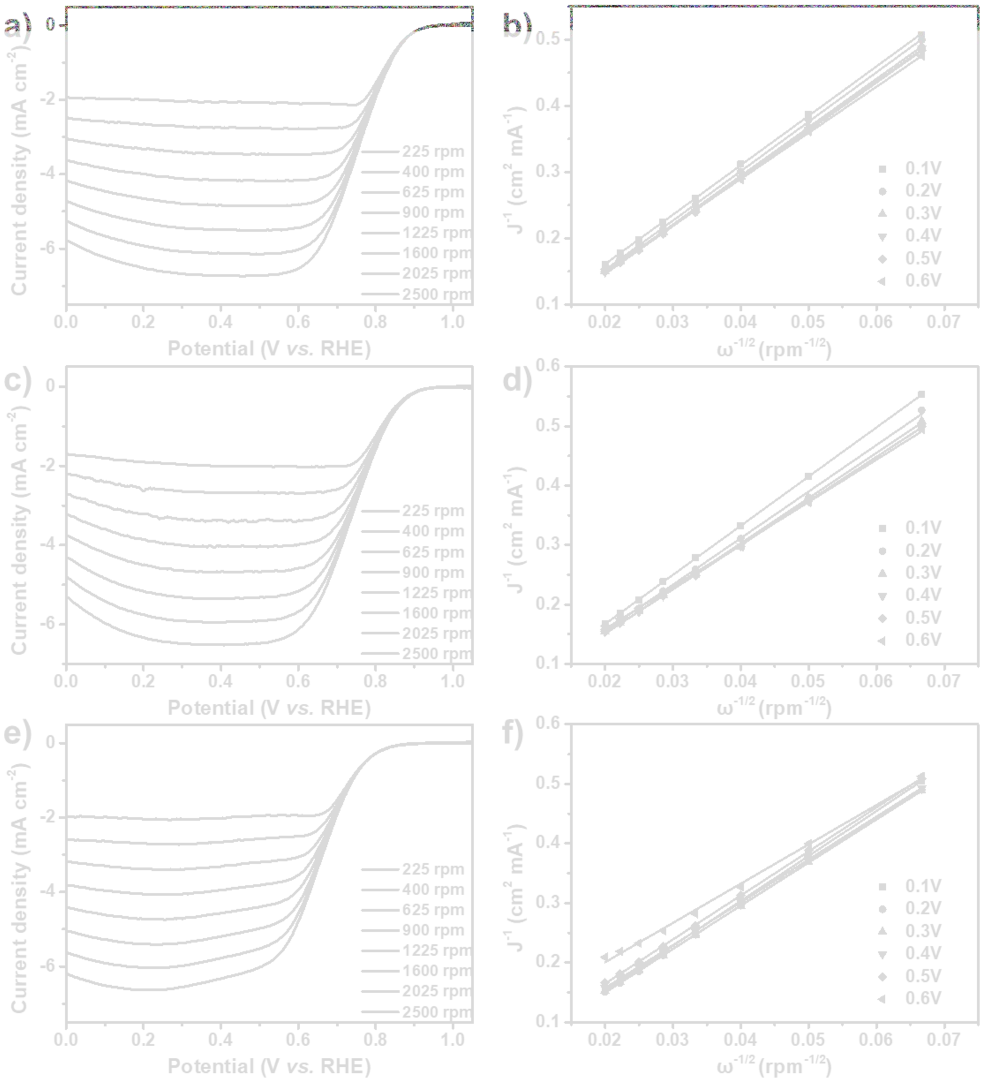

Figure S16. a) LSV curves at different rotation speeds (225–2025 rpm) and b) K-L plots of mPCN-Fe-800. c) LSV curves at different rotation speeds (225–2025 rpm) and d) K-L plots of mPCN-Fe. e) LSV curves at different rotation speeds (225–2025 rpm) and f) K-L plots of mPCN-Fe-1000.

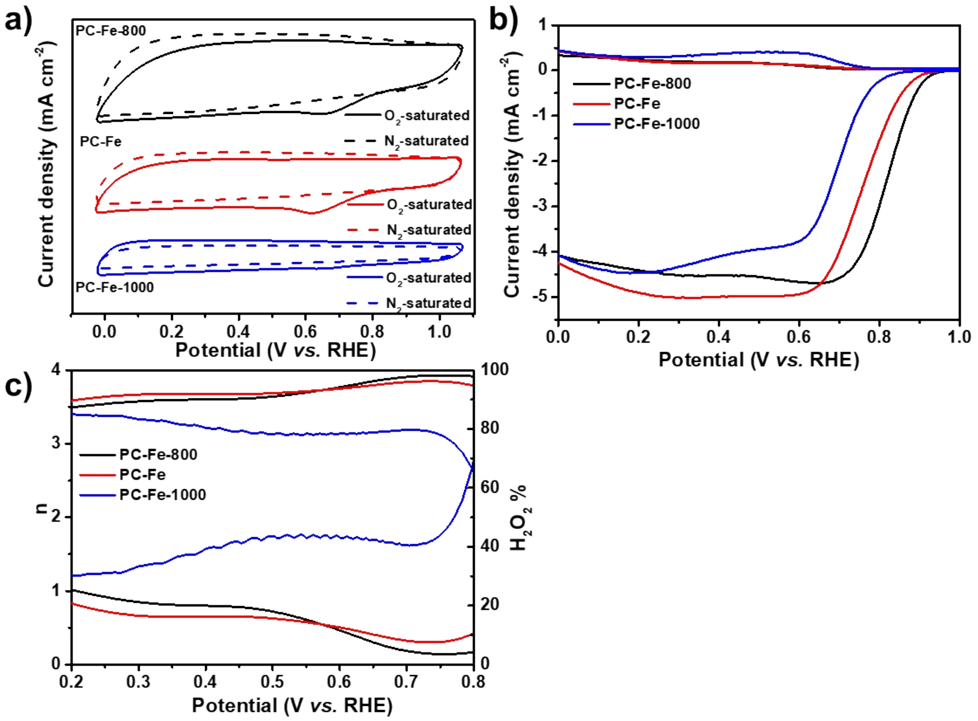

Figure S17. a) CV curves, b) RRDE curves and c) calculated electron transfer number and H_2O_2 yield of PC-Fe-800, PC-Fe, and PC-Fe-1000.

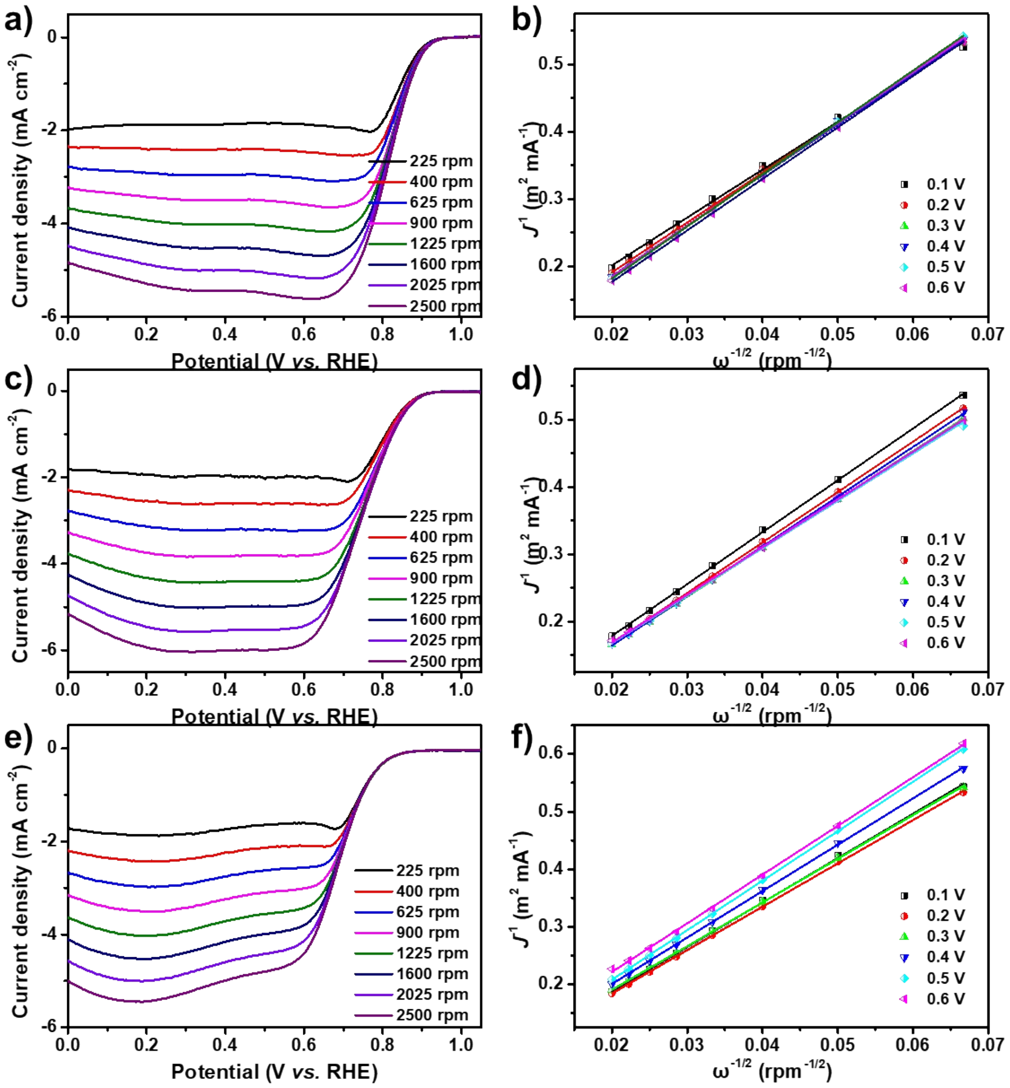

Figure S18. a) LSV curves at different rotation speeds (225–2025 rpm) and b) K-L plots of PC-Fe-800. c) LSV curves at different rotation speeds (225–2025 rpm) and d) K-L plots of PC-Fe. e) LSV curves at different rotation speeds (225–2025 rpm) and f) K-L plots of PC-Fe-1000.

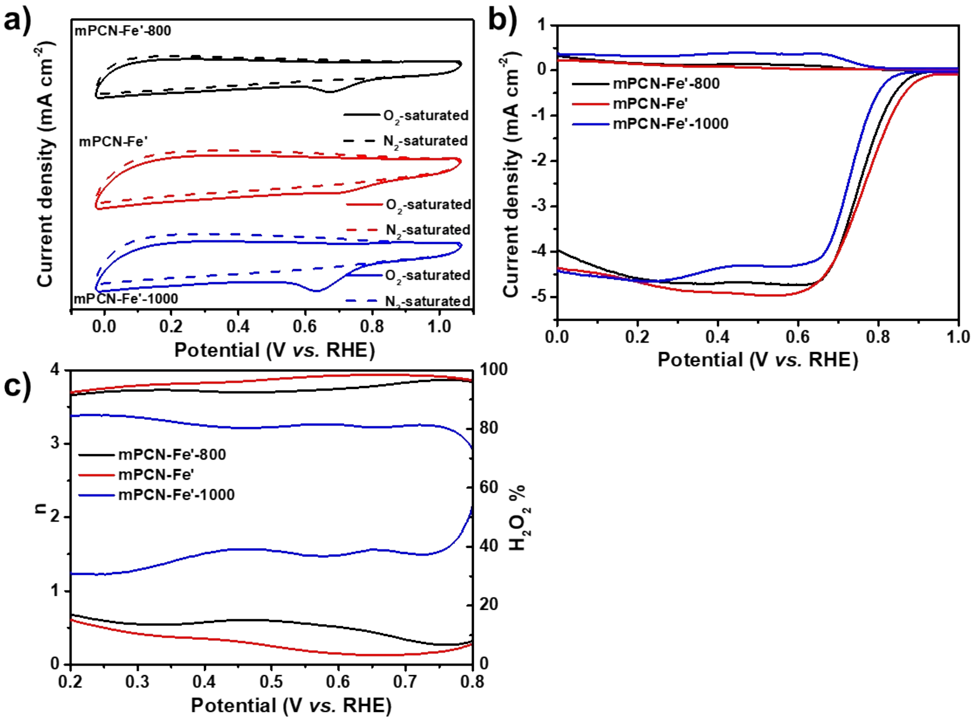

Figure S19. a) CV curves, b) RRDE curves and c) calculated electron transfer number and H_2O_2 yield of mPCN-Fe’-800, mPCN-Fe’, and mPCN-Fe’-1000.

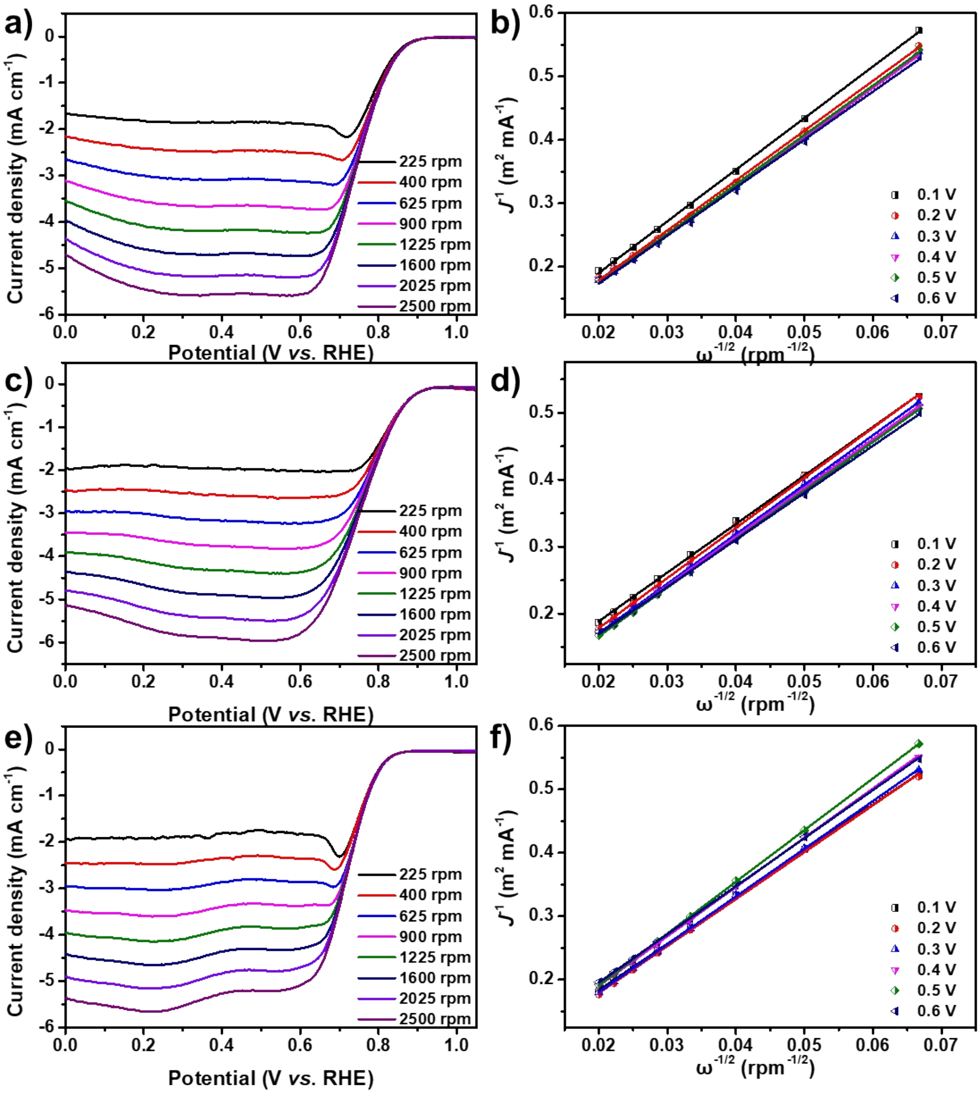

Figure S20. a) LSV curves at different rotation speeds (225–2025 rpm) and b) K-L plots of mPCN-Fe'-800. c) LSV curves at different rotation speeds (225–2025 rpm) and d) K-L plots of mPCN-Fe'. e) LSV curves at different rotation speeds (225–2025 rpm) and f) K-L plots of mPCN-Fe'-1000.

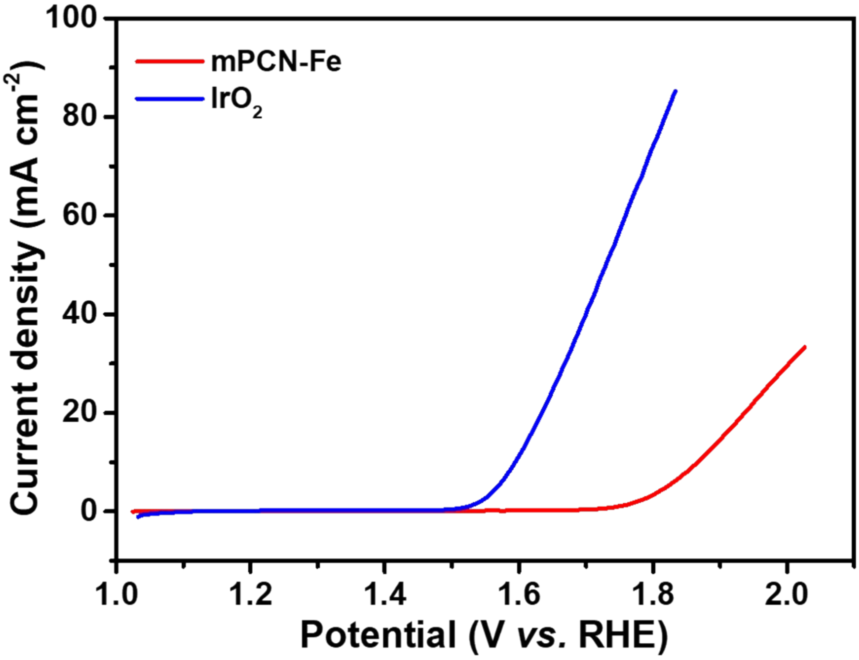

Figure S21. LSV curve of mPCN-Fe and IrO_2 in 1 M KOH in O_2-saturated solution.

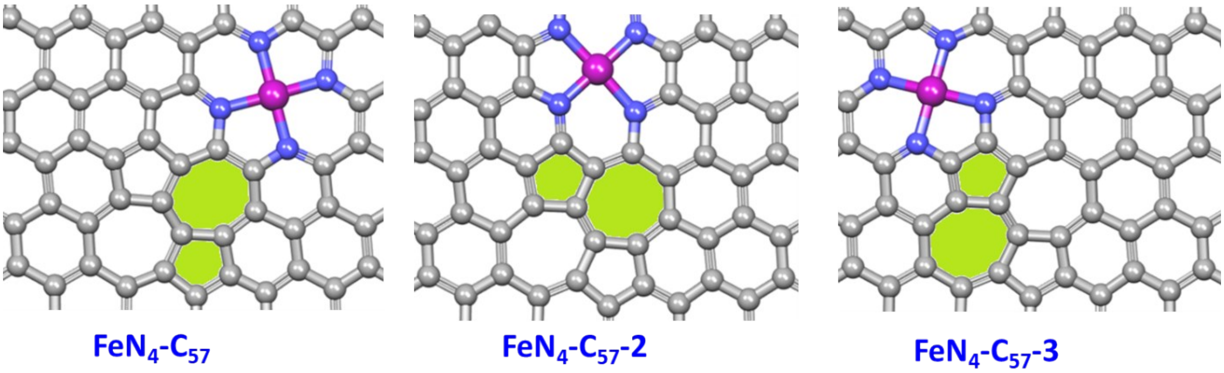

Figure S22. The representative FeN$_4$-C$_{57}$ models for DFT calculations: FeN$_4$-C$_{57}$ -1, FeN$_4$-C$_{57}$ -2 and FeN$_4$-C$_{57}$ -3.

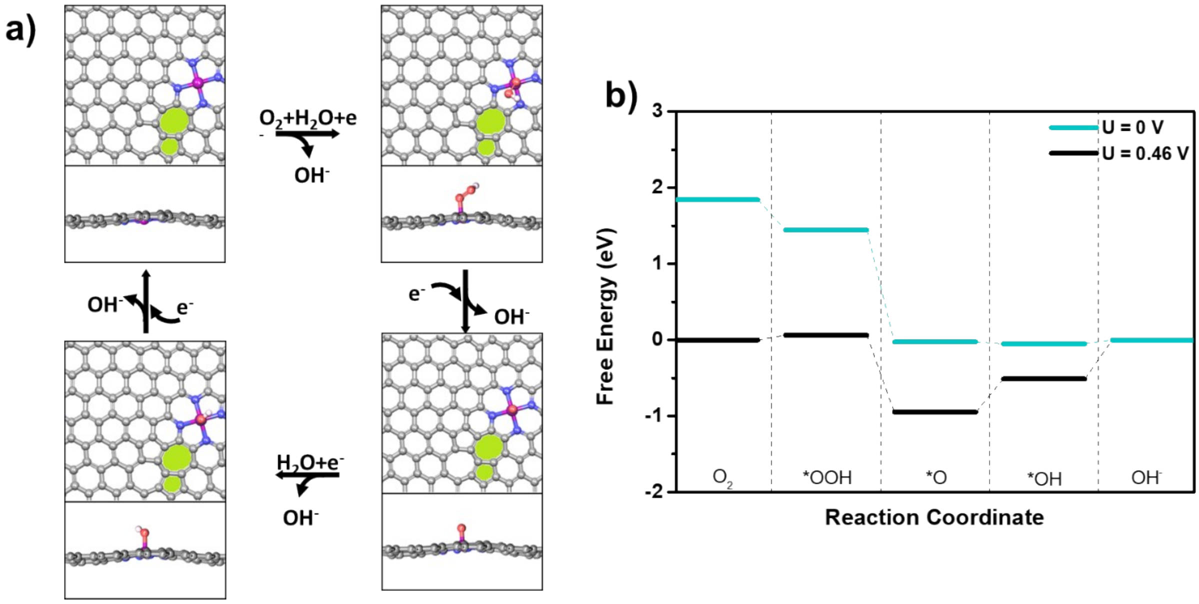

Figure S23. a) The catalytic mechanism scheme of FeN$_4$-C$_{57}$. b) Free energy diagrams of ORR on FeN$_4$-C$_{57}$ -1 at U=0 V and U=0.46 V.

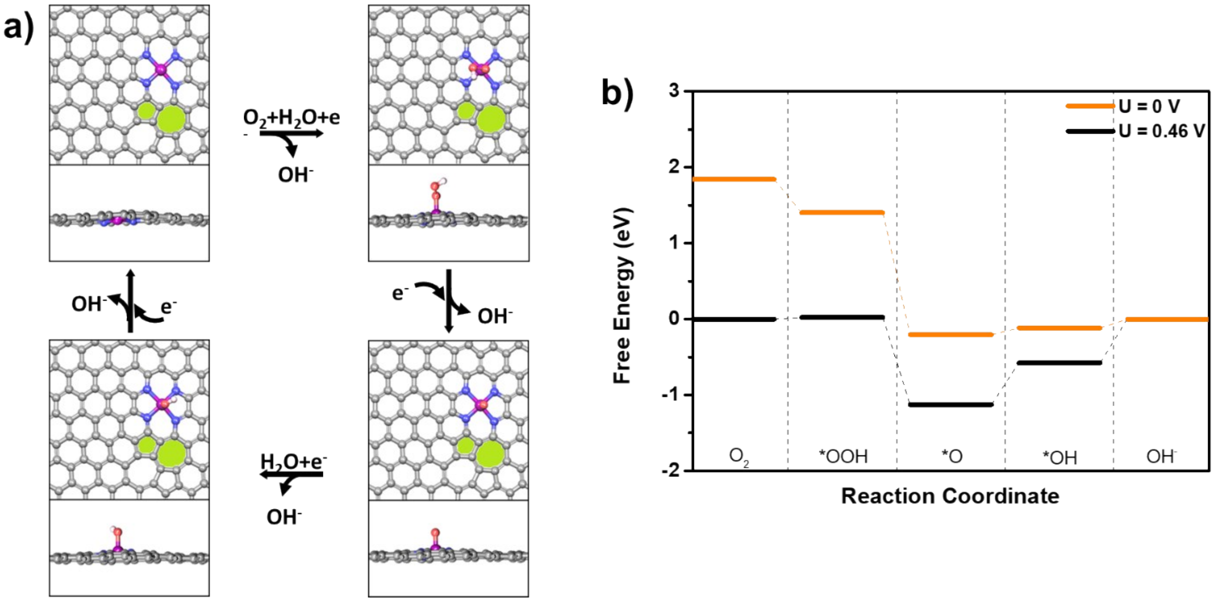

Figure S24. a) The catalytic mechanism scheme of FeN_4-C_{57} -2. b) Free energy diagrams of ORR on FeN_4-C_{57} -2 at U=0 V and U=0.46 V.

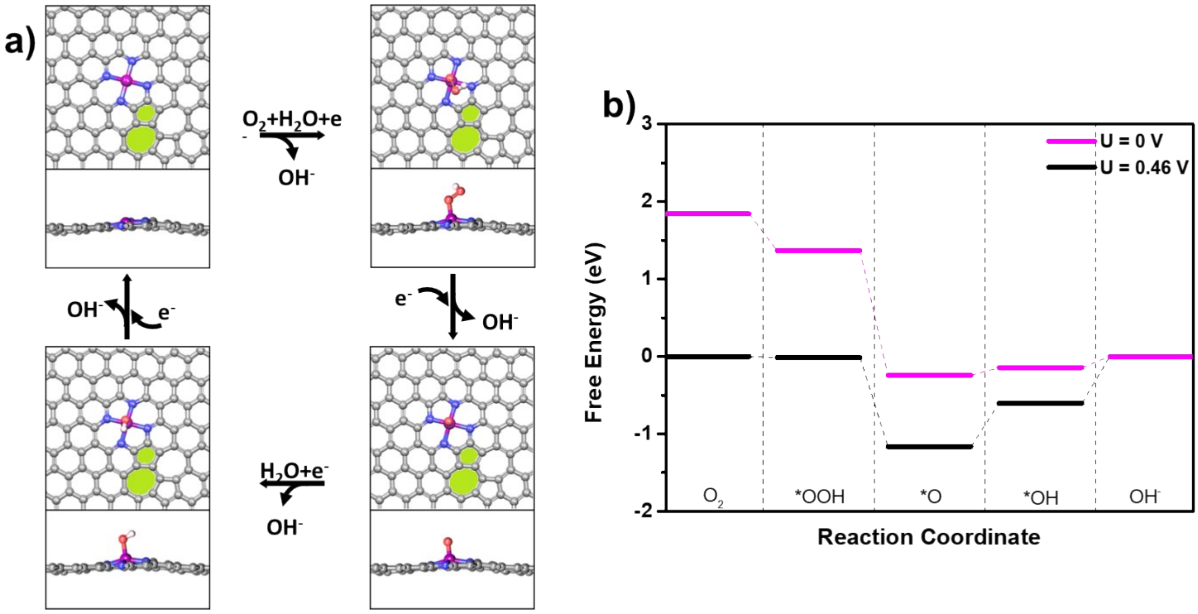

Figure S25. a) The catalytic mechanism scheme of FeN_4-C_{57} -3. b) Free energy diagrams of ORR on FeN_4-C_{57} -3 at U=0 V and U=0.46 V.

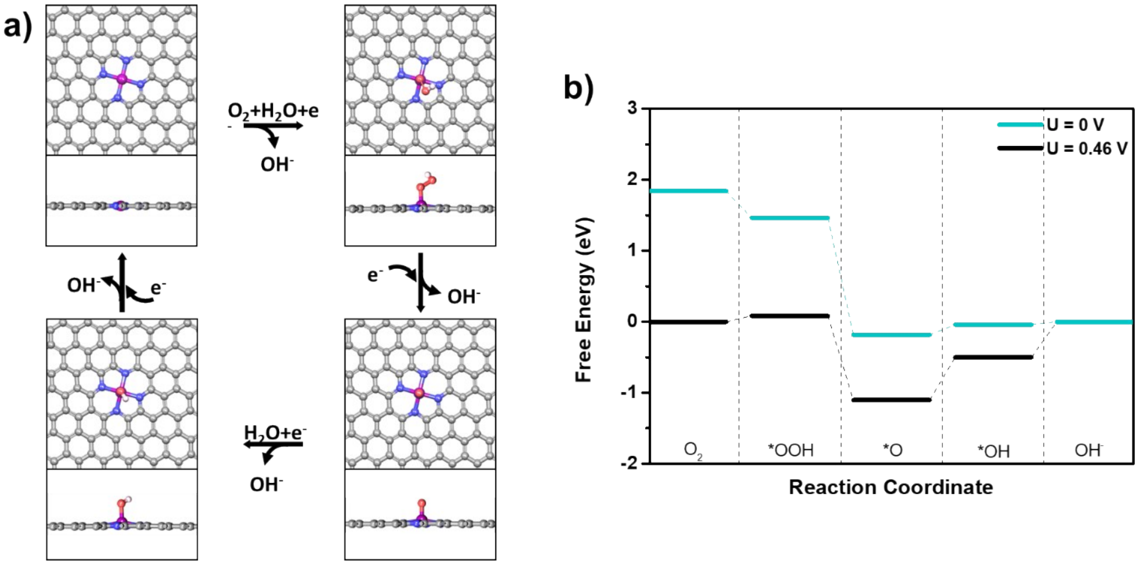

Figure S26. a) The catalytic mechanism scheme of FeN_4-C_{66}. b) Free energy diagrams of ORR on FeN_4-C_{66} at U=0 V and U=0.46 V.

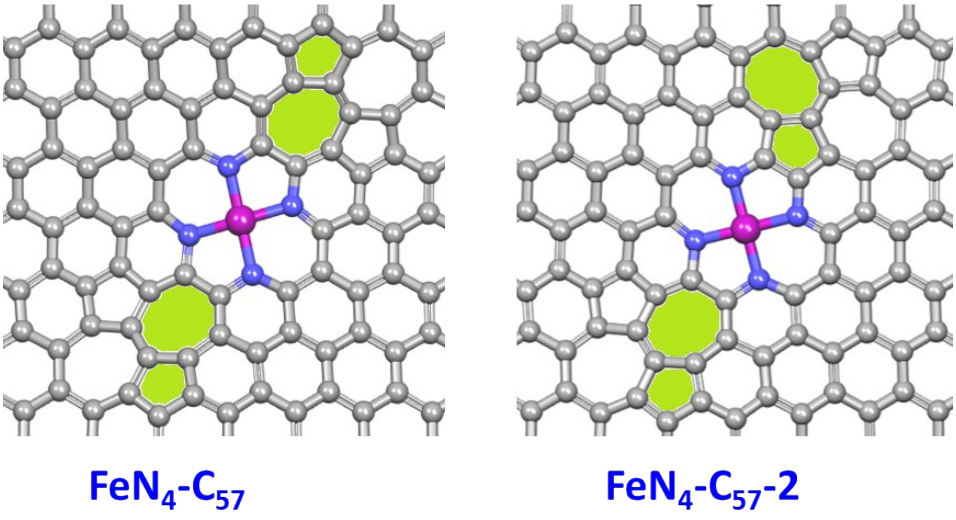

Figure S27 The representative FeN_4-$2C_{57}$ models for DFT calculations: FeN_4-$2C_{57}$ and FeN_4-$2C_{57}$ -2.

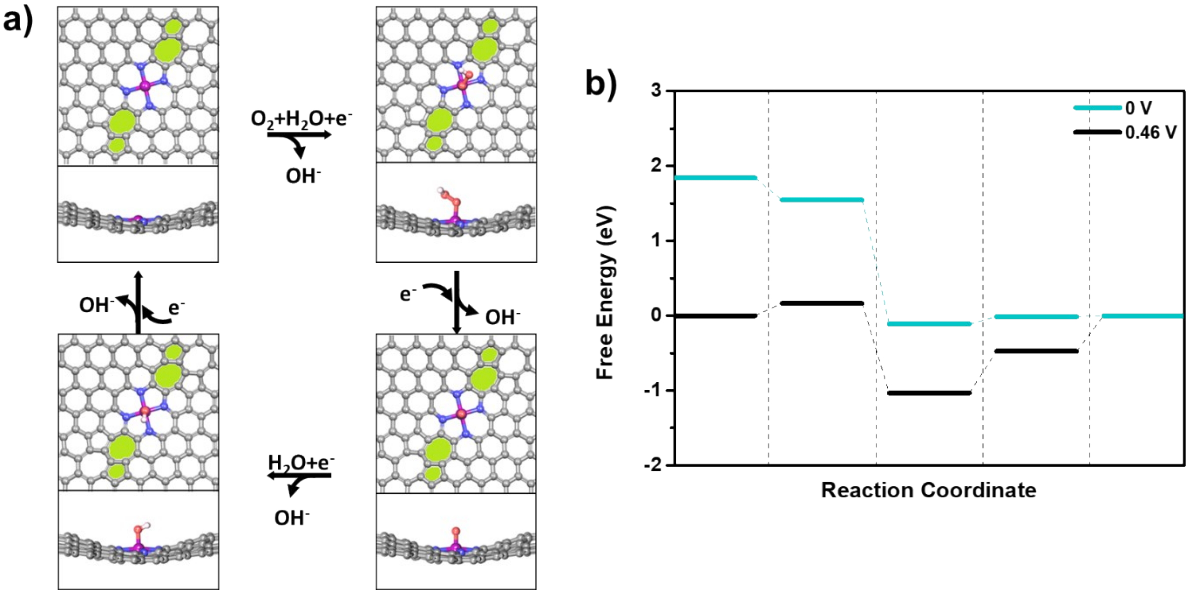

Figure S28. a) The catalytic mechanism scheme of FeN_4-$2C_{57}$. b) Free energy diagrams of ORR on FeN_4-$2C_{57}$ at U=0 V and U=0.46 V

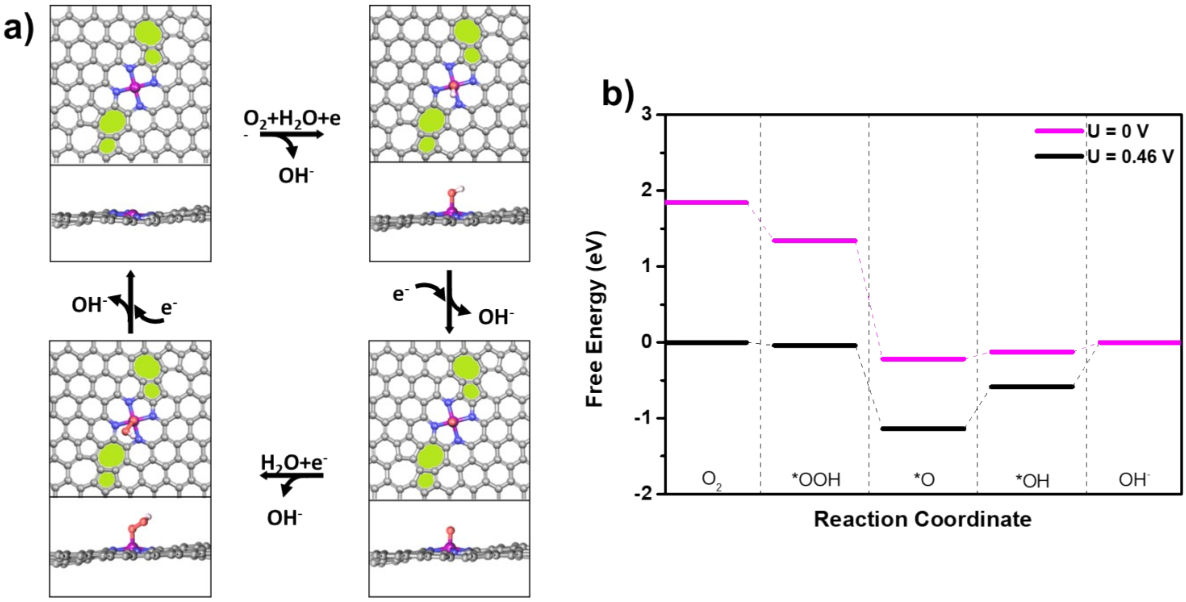

Figure S29. a) The catalytic mechanism scheme of FeN_4-$2C_{57}$-2. b) Free energy diagrams of ORR on FeN_4-$2C_{57}$ -2 at U=0 V and U=0.46 V.

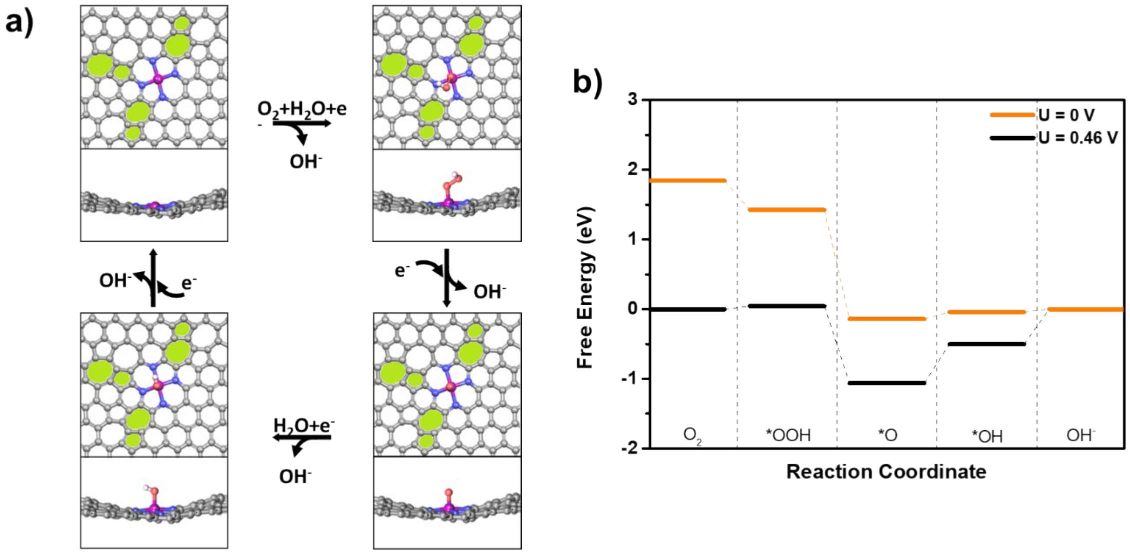

Figure S30. a) The catalytic mechanism scheme of FeN$_4$-3C$_{57}$. b) Free energy diagrams of ORR on FeN$_4$-3C$_{57}$ at U=0 V and U=0.46 V。

Table S1. Computed total energies (E^{DFT}) and thermodynamic quantities, for the gas phase CO_2, CO and H_2 species. (T = 298.15 K, P = 1 bar), and free H_2O at the 298.15 K, 0.035 bar.

	E^{DFT} (eV)	ZPE (eV)	TS (eV)	G (eV)
CO_2	-23.00	0.31	0.66	-23.35
CO	-14.80	0.14	0.67	-15.33
H_2O	-14.22	0.59	0.67	-14.30
H_2	-6.76	0.27	0.41	-6.90

Table S2. Comparison of ORR performance for mPCN-Fe with others reported Fe-N-C electrocatalysts.

Catalyst	Electrolyte	Half-wave potential (V vs. RHE)	Limiting current density (mA cm^{-2})	Reference
mPCN-Fe	0.1 M KOH	0.83	4.9	This work
	0.5 M H_2SO_4	0.64	4.9	
Fe-N-DSC	0.1 M KOH	0.84	4.5	ACS Nano. 2018, 12, 208−216
	0.5 M H_2SO_4	0.65	4.7	
Fe-N-doped carbon capsules	0.1 M KOH	0.83	4.6	ACS Nano. 2016, 10, 5922−5932
	0.5 M H_2SO_4	0.52	3.5	
Fe-N-doped carbon nanofibers	0.1 M KOH	0.82	5.2	Angew.Chem., Int.Ed. 2015, 127, 8297 –8301
Fe-N/C catalyst	0.1 M KOH	0.81	6	J. Am. Chem. Soc. 2014, 136, 11027−11033
	0.1 M $HClO_4$	0.60	6	
Fe-N doped hollow carbon-nanoshells	0.1 M KOH	0.85	5.2	ACS Catal. 2015, 5, 3887−3893

Table S3. Comparison of the Zn-air battery results with recent literature.

Catalysts	**Electrolytes**	**Battery performances**	**Reference**
mPCN-Fe	6 M KOH with 0.1 M $ZnCl_2$	1.51 V；153 mW cm^{-2}；681 mA h g^{-1}	This work
Fe−N/C−700	6 M KOH	1.5 V; 727 mAh g^{-1}；965 Wh kg^{-1}	Small 2016, 12, 41, 5710–5719
$Fe_aCo_{1-a}O_x$/NrGO hybrid	6 M KOH with 0.2 M $ZnCl_2$	1.44 V；86 mW cm^{-2}；756 mA h g^{-1}	Adv. Mater. 2017, 29, 1701410
Cu@Fe-N-C	6 M KOH with 0.2 M $ZnCl_2$	1.48 V；153.0 mW cm^{-2}	Adv. Funct. Mater. 2018, 28, 1802596
3D nanosheet-linked polyhedron carbon (NLPC)	6 M KOH	1.44 V；102 mW cm^{-2}；768 mA h g^{-1}	Adv. Funct. Mater. 2018, 28, 1705356
$NiCo_2O_4$ NPs	6 M KOH with 0.2 M $ZnCl_2$	1.49 V；103 mW cm^{-2}；403 mA h g^{-1}	Adv. Mater. 2018, 30, 1800005
Fe–N–C	6 M KOH with 0.2 M $Zn(CH_3COO)_2$	1.41V；149.4 mW cm^{-2}；663 mA h g^{-1}	Adv. Mater. 2018, 30, 1804504
N-doped carbon networks	6 M KOH with 0.2 M $ZnCl_2$	1.4V；55 mW cm^{-2}	Small 2018, 14, 1704169
CoFe/N-GCT	6 M KOH with 0.2 M $ZnCl_2$	1.43V；203 mW cm^{-2}；663 mA h g^{-1}	Angew.Chem., Int.Ed. 2018, 57,16166 –16170
S-GNS/$NiCo_2S_4$ nanocomposite	6 M KOH with 0.2 M $ZnCl_2$	1.35V；216.3 mW cm^{-2}；663 mA h g^{-1}	Adv. Funct. Mater. 2018, 28, 1706675

References

[1] T. Nozoe, S. Seto, S. Matsumura, Y. Murase, *Bull. Chem. Soc. Jpn.* **1962**, *35*, 1179.

[2] W. S. H. Jr, R. E. Offeman, *J. Am. Chem. Soc.* **1958**, *80*, 1339.

[3] W. Wei, H. Liang, K. Parvez, X. Zhuang, X. Feng, K. Müllen, *Angew. Chem., Int. Ed.* **2014**, *53*, 1570.